



Repositorio Institucional de la Universidad Autónoma de Madrid

<https://repositorio.uam.es>

Esta es la **versión de autor** del artículo publicado en:

This is an **author produced version** of a paper published in:

Biosensors and Bioelectronics 74 (2015): 1069 - 1075

DOI: <http://dx.doi.org/10.1016/j.bios.2015.08.002>

Copyright: © 2015 Elsevier

El acceso a la versión del editor puede requerir la suscripción del recurso

Access to the published version may require subscription

Immunosensing platform based on gallium nanoparticle arrays on silicon substrates

Antonio García Marín,^a María Jesús Hernández,^a Eduardo Ruiz,^a Jose María Abad,^b
Encarnación Lorenzo,^{b*} Juan Piqueras,^a Jose Luis Pau^a

Affiliations

^aGrupo de Electrónica y Semiconductores, Departamento de Física Aplicada, Universidad Autónoma de Madrid, Cantoblanco, 28049 Madrid, Spain

^bDepartamento de Química Analítica y Análisis Instrumental, Universidad Autónoma de Madrid, Cantoblanco, 28049 Madrid, Spain

Corresponding author:

*Email: encarnacion.lorenzo@uam.es

Abstract

Gallium nanoparticles (GaNPs) of different sizes are deposited on Si(100) substrates by thermal evaporation. Through ellipsometric analysis, it is possible to investigate the plasmonic effects in the GaNPs and exploit them to develop biosensors. The excitation of the resonant modes for certain incidence angles leads to negative values of the imaginary part of the pseudodielectric function (ϵ_i) obtained in ellipsometry. Furthermore, there is an abrupt sign change when the difference between the phase shifts of p- and s- polarization components reaches 180° at an energy of around 3.15 eV. At that energy, reversal of the polarization handedness (RPH) occurs for an elliptically-polarized input beam. The energy of the RPH

condition reduces as the evaporation time increases. The slope of $\langle \varepsilon_i \rangle$ at the RPH condition is extremely sensitive to changes in the surrounding medium of the NP surface and prompts the use of the GaNP/Si system as sensor platform. Fourier transformed infrared spectroscopy (FTIR) is used before and after functionalization with 3,3'-dithiodipropionic acid di(N-succinimidyl ester) and a glutathione-specific antibody to confirm the chemical modification of the sample surface. The developed immunosensor is exposed to different concentrations of glutathione (GSH) showing a linear relationship between the slope of the pseudodielectric function at the RPH condition and the GSH concentration. The immunosensor shows a limit of detection of 10 nM enabling its use for the detection of low GSH levels in different medical conditions.

Keywords: localized surface plasmon resonance (LSPR), spectroscopic ellipsometry, gallium nanoparticles, immunosensor, glutathione

1. Introduction

Surface plasmons are collective oscillations of free electrons in the vicinity of metal surfaces. Their use for the fabrication of sensors and biosensors has been studied for several decades, focusing most of the studies, on the excitation of plasmons in thin films and nanostructures of noble metals (Homola et al. 1999; Schasfoort and Tudos 2008). Many sensors have been developed employing different coupling systems (prisms, gratings and optical waveguides) to satisfy the dispersion relation of those waves in metallic thin films (Homola 2003). With the advent of nanotechnology, the use of nanostructures has become more common due to the possibility of enhancing the sensitivity at the nanoscale, as well as the level of integration. In addition, the confinement of the electric field vibrations in a small volume can

be achieved by simpler coupling methods, what is an advantage for the design of the sensing platforms (Aćimović et al. 2014).

Many studies on the localized surface plasmon resonance (LSPR) of metal nanostructures have focused on gold (Au) and silver (Ag), whose resonance energies are found in the IR-visible wavelength range (Eustis and El-Sayed 2006; Viswambhari Devi et al. 2015; Willets and Duyne 2007). However, low melting point metals such as gallium (Ga) have been less studied. During the last years, there has been an increasing attention to nanostructures based on Ga because of the wide tunability of the resonance energy from the UV to the IR spectral region, the simplicity of the preparation methods, the resilience of the metal plasmon to the oxidation in ambient conditions, the spectral splitting of its resonant modes due to the hemispherical geometries, and the dependence of the oscillatory modes on the polarization of the incident light (Albella et al. 2011; Wu et al. 2007). Thanks to those properties, their effective use have been demonstrated in different applications, such as Surface-Enhanced Raman Spectroscopy (SERS), fluorescence spectroscopy, and photo-induced degradation studies of biomolecules, showing large UV local enhancement factors compared to Au or Ag nanoparticles (Yang et al. 2013).

One interesting feature of LSPRs is the possibility to enhance the sensitivity in optical sensing systems (Lodewijks et al. 2012; Michieli et al. 2015). GaNPs present two oscillatory modes at different energies due to the hemispherical geometry of the NPs (Tonova et al. 1999). Those modes give rise to two significant bands in the pseudodielectric function obtained by external reflection ellipsometry at incidence angles of around 70°. Ga deposition often produces a bimodal distribution with large GaNPs surrounded by smaller ones. This work analyzes their optical properties by changing the incidence angle. The study shows evidence of a characteristic behavior of the pseudodielectric function when the p-component of the reflected

beam retards with respect to the s-component. This effect leads to a reversal of polarization handedness (RPH).

Furthermore, to demonstrate the possibility of using the RPH condition in Ga plasmonic structures for sensing purposes, an immunosensor for glutathione (GSH) is proposed. GSH is a small biomolecule, present in all living organisms, but predominantly in eukaryotic cells (Hedley and Chow 1994; Meister 1983), which plays a critical role in numerous biological processes (Meister and Anderson 1983; Sies 1999). Among the wide number of roles, intracellular redox balance (Gutscher et al. 2008) detoxification, modulation of the immune response (Buttke and Sandstrom 1994), protein folding (Appenzeller-Herzog 2011), and transport of organic sulfur (May et al. 1998) can be highlighted. Low levels of GSH are related to several diseases, such as Crohn's disease, Alzheimer (Pocernich and D. A. Butterfield 2012), cancer (Lusini et al. 2001), inflammatory (Ruan et al. 1997), immune (Galera et al. 1996), and metabolic diseases (Mayatepek and Jaeken 2012; Meister 1988).

Some studies reveal reductions of GSH in the human body related to different diseases. Typically, the GSH concentration is found to be 3.24 μM in plasma and 4.35 μM in serum (Galera et al. 1996; Morrison et al. 1999). A reduction of 22% of GSH in plasma (from 3.24 μM to 2.46 μM) is found to be related to human immunodeficiency virus (HIV). On the other hand, a reduction of 26% of GSH in serum (from 4.35 μM to 3.20 μM) is found in patients of parental coronary heart disease.

In ulcerative colitis, tissue GSH levels drop about 54% in the mucosal-submucosal layer (from 614 ± 126 to 283 ± 71 nmoles/g wet tissue), and 52% in the muscularis externa layer (from 837 ± 130 to 398 ± 98 moles/g wet tissue) (Ruan et al. 1997). For Crohn's colitis, the tissue GSH levels are found to be 337 ± 139 nmoles/g for the mucosal-submucosal layer and 393 ± 147 nmoles/g in the muscularis externa layer, involving GSH reductions of 45% and 53%, respectively.

Although intracellular GSH concentrations in serum and plasma are in the micromolar range, GSH sensing in other applications may require higher sensitivity. Standard kits usually rely on spectrofluorimetry (Meyer et al. 2001; Xu et al. 2015) and ELISA (antigen-antibody recognition) and reach limits of detection around 0.1-0.5 $\mu\text{g/mL}$ (0.325-1.625 μM). Other techniques such as electrochemistry (Harfield et al. 2012; Ndamaniha et al. 2009; White et al. 2002), high-performance liquid chromatography (Lu et al. 2007; Vacek et al. 2006; Zhang et al. 2005), gas chromatography (Kataoka et al. 1995), or quartz crystal microbalance (Gordon et al. 2005) have been employed enabling the detection at lower levels. However, all these methods have advantages but also drawbacks, such as less selectivity against other aminoacids or the time consuming characteristics, that make the analysis tedious and complicated.

In this work, an immunosensor for GSH is developed by functionalizing the GaNPs, previously deposited by thermal evaporation on Si substrates, with a GSH-specific antibody. This procedure to deposit GaNPs on substrates has arisen as a cost-effective and fast process to produce intense surface plasmonic resonances (Hernández et al. 2010). The immunosensor is based on the quantification of the spectral changes observed in the pseudodielectric function obtained from spectroscopic ellipsometry around the RPH condition. The concentration of GSH is determined by exposition of this immunosensing platform to different concentrations of GSH from the nanomolar to the submicromolar range. The limits of detection achieved compare favorably with other methods for GSH determination.

2. Materials and Methods

2.1. Materials

L-reduced glutathione, 3,3'-dithiodipropionic acid di(N-succinimidyl ester) (DTSP), acetone, dimethyl sulfoxide (DMSO) and potassium chloride (KCl) are purchased from Sigma-Aldrich (St. Louis, MO). GSH polyclonal antibody (anti-GSH) is acquired from Abcam (U.K.).

99.9999% pure gallium (Ga) is acquired from Goodfellow (England). All chemicals are used as received without further purification. All solutions are prepared with ultrapure water (18 M Ω ·cm) obtained from a Direct-Q 3 UV Millipore purification system.

2.2. Gallium nanoparticles (GaNPs) deposition

GaNPs are obtained by depositing Ga on Si(100) wafers in a Joule-effect thermal evaporator under a constant electrical current at different times, from 0.5 to 2.5 minutes. Prior to Ga deposition, substrates are cleaned with a water diluted hydrofluoric acid solution to etch the native oxide. The substrate is ice-cooled in order to keep the sample temperature near zero degrees Celsius. This prevents unintentional heating effects during evaporation and reduces surface migration and coalescence of droplets induced by the minimization of surface free energy in the NPs (Wu et al. 2009). A NP-covered area of 20 cm² is obtained from a single evaporation. The sample is then cleaved into different chips of about 0.4 cm² for its use in further experiments.

2.3. GaNPs/Si surface characterization

The morphology of the GaNPs/ Si surface is studied using a field-effect scanning electron microscopy (SEM) at 10 kV with an Everhart-Thornley secondary-electron detector.

Fourier transform infrared measurements are performed in a FTIR Bruker IFS66v spectrometer with a diffuse reflection accessory.

Ellipsometric measurements are carried out by using a Jobin Yvon UVISSEL spectroscopic phase-modulated ellipsometer in external reflection mode. Modulator and analyzer angles are set at 0 and 45°, respectively. Incidence angles between 70 and 45° and energies between 1.5 and 4.5 eV are used for the present work. The light spot has an elliptical shape with a 7.0 mm×4.0 mm size for an incidence angle of 70°, and a 6.6 mm×4.0 mm size, at 45°.

2.4. GaNP/Si immunosensor development

GaNPs/Si based immunosensors are developed following the procedure previously described with slight modifications (García-Marín et al. 2014). Prior to the functionalization, the GaNPs/Si chips are carefully selected, by measuring the imaginary part of the pseudodielectric function (ϵ_i) spectra to have the same peak-to-peak amplitude and RPH energy. Then, the GaNPs/Si surface is functionalized with a thiol monolayer. For this purpose, the sample is immersed in a 4 mM solution of DTSP in DMSO and left overnight. This gives rise to the chemical modification of the GaNPs/Si surface with an “activated ester” termination, which can react with the primary amino groups present in the antibody, enabling covalent bonding through the formation of amide bonds (Darder et al. 1999; Wagner et al. 1996). Then, the DTSP-modified GaNPs/Si surface is rinsed with acetone and blown with dry nitrogen. The next step comprises the immobilization of an antibody specific to GSH on the DTSP-functionalized GaNPs/Si surface by incubation of the chip in 0.01 M KCl containing the antibody for 2 hours. Then, the chip is soaked into 0.01 M KCl solution for 1 hour to remove not covalently bound molecules of anti-GSH. Finally, the developed immunosensor chips are rinsed with deionized water and blown with dry nitrogen.

The optimal antibody concentration is studied by using increasing concentrations of anti-GSH and recording the energy redshift produced in ϵ_i which is proportional to the surface coverage. The resulting curve is optimally fitted by using the Langmuir isotherm equation (Equation 6).

2.5. Immunosensor ellipsometric response

GSH recognition is performed by incubation of immunosensor chips for 1 hour in aqueous solutions containing increasing concentrations of GSH between 50 and 800 nM. Afterwards, the surface is washed with deionized water and gently blown with dry nitrogen. After the

incubation step, the chip is re-measured in the ellipsometer to record $\langle \varepsilon_i \rangle$ at the same conditions describe above.

3. Results and discussion

3.1. Nanoparticle characterization

Ga is deposited on Si(100) wafers as described in the Experimental Section. The average GaNP size can be controlled by the deposition time. The as-evaporated NPs on the Si substrate are observed using scanning electron microscopy (SEM). As can be seen in **Fig. 1a**, the Si surface is fully covered by NPs of different sizes. The NP coalescence process leaves behind a halo of smaller NPs between the largest ones, giving rise to a bimodal NP size distribution (**Fig. 1b**). The mechanism for the formation of GaNPs is based on the Ostwald ripening process, which comprises the growth of large NPs from the smaller ones as the evaporation time increases (Campbell 1997). The histogram shows that the number of small NPs strongly increases as the diameter reduces. The average size of the very small NPs remains fairly constant with the evaporation time. Furthermore, a high number of particles is found between 200 and 300 nm in diameter yielding an average size of 240 nm in that range. This average size changes with the evaporation time. The interparticle distance between the largest NPs is estimated to be around 80 ± 30 nm. From the cross-sectional image (**inset of Fig. 1a**), we observe that the NP contact angle on the substrate plane is close to 90° , giving rise to hemispherical shapes. This morphology results from the surface tension of liquid Ga on the silicon substrate, and it is preserved during the functionalization works due to the formation of a thin oxide film on the NP surface (Knight et al. 2015; Wu et al. 2009).

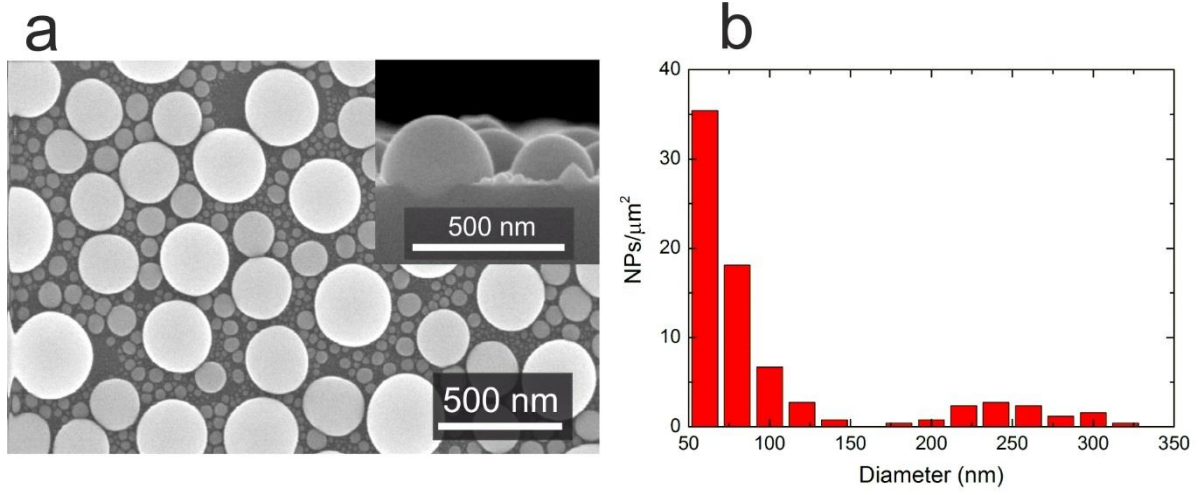


Fig. 1. SEM images of the as-deposited GaNPs for a 2-min evaporation time at a magnification of 100.000× (a) and the corresponding histogram for this sample (b). The inset of Fig. 1a is a cross-section image of the GaNPs at 100.000x.

3.2. Ellipsometric determination of potential amplification at as-deposited GaNPs

The experimental setup employed is represented in **Fig. 2a**. Ellipsometric functions ψ (Ψ) and δ (Δ), for GaNPs/Si(100) systems are obtained in the 1.5-4.5 eV range and are defined through (Tompkins 1993):

$$\rho = R_p / R_s = \tan \Psi \cdot \exp(i \cdot \Delta) \quad (1)$$

where ρ is the ratio between the R_p and R_s reflection coefficients for light polarized parallel (p) and perpendicular (s) to the plane of incidence. The tangent of Ψ is defined as the ratio between the reflection coefficients for the p- and s- polarization components of the reflected beam. Δ is the difference between the phase shifts for both polarization components. This parameter seems to have a relevant role for arrays of plasmonic nanostructures because of its large variation in resonant conditions, which makes it very sensitive to changes in the surrounding medium (Lodewijks et al. 2012). In air ambient ($n = 1$), the pseudodielectric function ($\langle \epsilon \rangle$) is related to those parameters through:

$$\langle \varepsilon \rangle = \langle \varepsilon_r \rangle + i \langle \varepsilon_i \rangle = \sin^2(\varphi) \cdot \left(1 + \tan^2(\varphi) \cdot \frac{(1-\rho)^2}{(1+\rho)^2} \right) \quad (2)$$

$$\langle \varepsilon_r \rangle = \sin^2(\varphi) \cdot \left(1 + \frac{\tan^2(\varphi) \cdot (\cos^2(2\Psi) - \sin^2(\Delta) \cdot \sin^2(2\Psi))}{(1 + \sin(2\Psi) \cdot \cos(\Delta))^2} \right) \quad (3)$$

$$\langle \varepsilon_i \rangle = \frac{\sin^2(\varphi) \cdot \tan^2(\varphi) \cdot \sin(4\Psi) \cdot \sin(\Delta)}{(1 + \sin(2\Psi) \cdot \cos(\Delta))^2} \quad (4)$$

where φ is the incidence angle. Real and imaginary parts of Equation 2 are defined in Equations 3 and 4, respectively (Tompkins 1993). When it is extended to more complex systems, such as multilayers or material islands on a substrate, these functions account for the properties of the whole system from the ellipsometric viewpoint. In previous works on GaNPs systems, the $\langle \varepsilon_i \rangle$ has been used to monitor the plasmonic resonance of these particles (Tonova et al. 1999; Wu et al. 2009). The spectra in **Fig. 2b** show the $\langle \varepsilon_i \rangle$ as a function of energy for different average sizes of NPs, obtained at an incidence angle of 70°. Due to the hemispherical geometry of the large GaNPs, the spectra exhibit two resonant modes as two broad bands separated several electronvolts (Tonova et al. 1999). The high energy band is found in the UV/visible range, whereas the low energy band comes out in the visible/IR range. Both modes follow a rather linear relationship between the resonance energy and the NP size (see **Fig. S1** in Supporting Information to compare our results with other authors). In general, the resonance energy decreases as the NP becomes larger allowing the tunability of the resonance in a wide range. For the largest NP sizes (diameter > 90 nm; red, black and magenta curves in **Fig. 2b**), the low energy modes are below the spectral range of our ellipsometric setup.

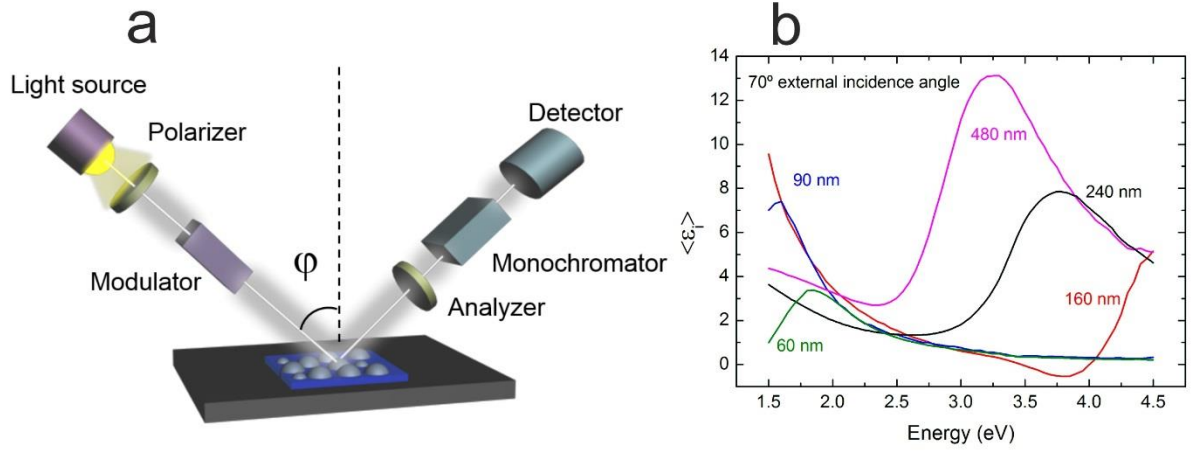


Fig. 2. (a) Scheme of the ellipsometric setup; (b) $\langle \epsilon_i \rangle$ obtained by illumination at the Si Brewster's angle (70°) for different average sizes for the large NPs, estimated from SEM images.

As the incidence angle is reduced, a characteristic line-shape is observed in $\langle \epsilon_i \rangle$ between both resonances, but closer to the higher energy mode (**Fig. 3a**).

To deepen into the understanding of the line-shape origin, the corresponding Ψ and Δ functions for these incidence angles are also shown in **Fig. 3b**. As the photon energy increases, from 1.5 eV, Ψ value decreases and a large phase variation in Δ can be observed associated to the retardation of the p-polarized component with respect to the s-polarized one. This variation yields a phase shift difference of 180° between both polarization components at high energies (around 3.00 and 3.25 eV, depending on the incidence angle), which gives rise to the RPH condition. For that phase shift difference, the reflected beam has a polarization vector that rotates in the opposite direction to the polarization vector of the elliptically-polarized incident beam. Between the energy of the Ψ dip and the RPH condition $\Delta = 180^\circ$, $\langle \epsilon_i \rangle$ takes negative values. At $\Delta = 180^\circ$, $\langle \epsilon_i \rangle$ presents a steep increase (**Fig. 3a**) due to the reduction of the denominator in Equation 4. The closer to zero is this denominator, the larger is the peak-to-peak amplitude shown by $\langle \epsilon_i \rangle$ around the RPH condition. If Ψ approaches 45° in this

RPH condition, $\sin(2\Psi) \cdot \cos(\Delta)$ becomes -1, and the denominator in Equation 4 is null. Therefore, a singularity is found in $\langle \varepsilon_i \rangle$. From a physical point of view, that means that the incident beam was circularly polarized and the reflected beam would present a polarization vector that would also rotate circularly in the opposite direction. **Inset of Fig. 3a** shows a representation of this effect.

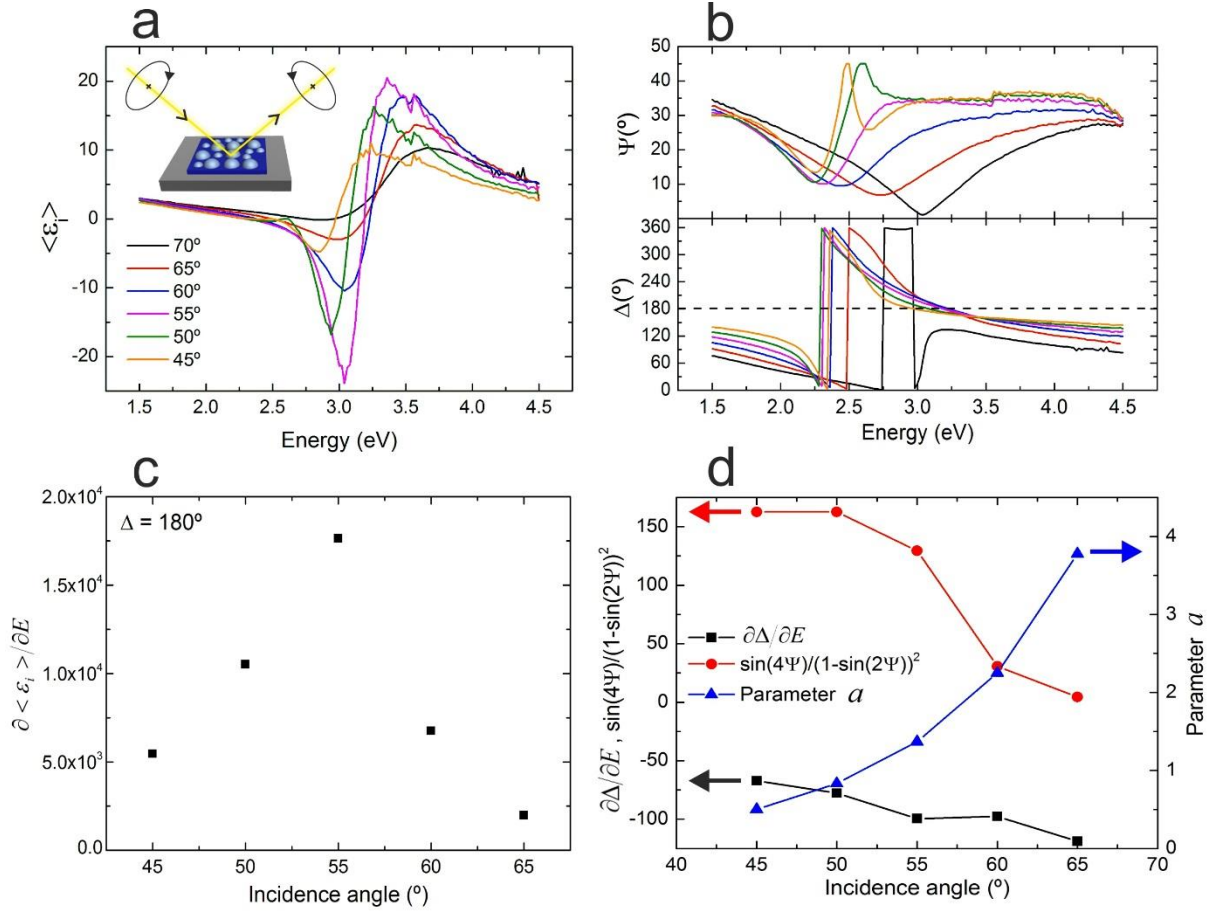


Fig. 3. (a) $\langle \varepsilon_i \rangle$, (b) Ψ and Δ at incidence angles between 70 and 45° for a GaNP sample with an estimated average size of 240 nm for the largest NPs. The RPH condition occurs at $\Delta = 180^\circ$, an angle highlighted with a horizontal dashed line; (c) $\partial \langle \varepsilon_i \rangle / \partial E$ at the RPH condition as a function of the incidence angle; (d) a representation of the different factors of Equation 5. Inset of Figure 3a shows a sketch of the inversion of the polarization handedness for a circularly-polarized beam upon reflection on the GaNPs/Si surface.

To study the influence of Ψ and Δ functions over $\langle \varepsilon_i \rangle$ at the RPH condition, Equation 4 is differentiated with respect to energy (E). The result is shown in:

$$\left. \frac{\partial \langle \varepsilon_i \rangle}{\partial E} \right|_{\Delta=180^\circ} = \frac{\partial \langle \varepsilon_i \rangle}{\partial \Psi} \cdot \frac{\partial \Psi}{\partial E} + \frac{\partial \langle \varepsilon_i \rangle}{\partial \Delta} \cdot \frac{\partial \Delta}{\partial E} = \frac{-a \cdot \sin(4\Psi)}{(1 - \sin(2\Psi))^2} \cdot \frac{\partial \Delta}{\partial E} \quad (5)$$

where $a = (\sin(\varphi)\tan(\varphi))^2$ and only depends on the incidence angle. A representation of Equation 5 versus the incidence angle is shown in **Fig. 3c**. $\partial\Delta/\partial E$ values are obtained after differentiating Δ curves around the RPH condition (**Fig. 3b**). As can be seen, the maximum value is obtained at 55° , following the similar trend observed in **Fig. 3a**, in which the largest variation of $\langle \varepsilon_i \rangle$ with respect to the energy is observed at the same incidence angle. As can be seen, Equation 5 can be separated into three different parts: a , $\sin(4\Psi)/(1 - \sin(2\Psi))^2$, and $\partial\Delta/\partial E$. **Fig. 3d** shows the different trends as a function of the incidence angle.

Fig. 4 shows $\langle \varepsilon_i \rangle$ for different evaporation times around the RPH condition. The inset shows two SEM images of GaNP samples obtained for evaporation times of 1 and 2 minutes. As can be seen, the line-shape shifts towards lower energies as evaporation time increases due to the larger NP size. The peak-to-peak amplitude reduces for evaporation times of 2.5 and 0.5 minutes. It is worth noting that samples obtained at evaporation times shorter than 0.5 minutes do not show evidence of the RPH condition in this spectral range.

Ellipsometric studies in arrays of small AgNPs (average sizes and interparticle distances of 11 and 3 nm, respectively) show a similar line-shape in $\langle \varepsilon_i \rangle$ but with a lower peak-to-peak amplitude (Verre et al. 2013).

From these studies, it is concluded that, for sensing purposes, an incidence angle of 55° and evaporation times of around 2 minutes (average size of 240 nm for the large NPs, as discussed above) will be used to maximize the peak-to-peak amplitude around the RPH condition in GaNP/Si systems. In further experiments, we use two parameters: the maximum

slope around the RPH condition (θ) and the energy shift (δE) of that maximum after the modification of the surface. Both of them can be extracted from $\langle \varepsilon_i \rangle$ spectra after its differentiation with respect to energy.

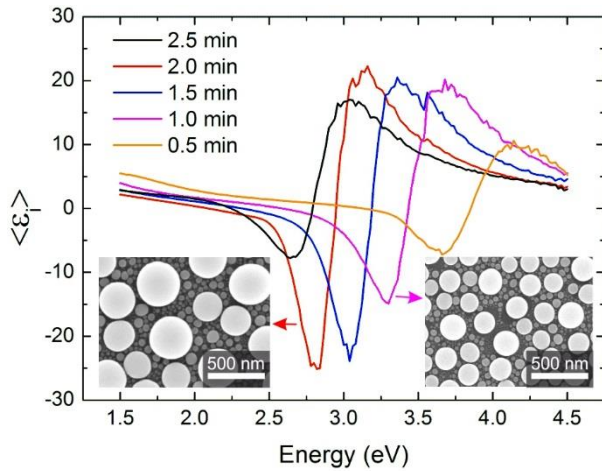


Fig. 4. $\langle \varepsilon_i \rangle$ for different samples obtained at different evaporation times and measured at an incidence angle of 55° . Insets show SEM images of NP samples obtained for evaporation times of 1 and 2 minutes.

3.3. Ellipsometric immunosensor based on gallium nanostructured surfaces

As it is described in the Experimental Section, the first step for immunosensor development consists in the functionalization of the GaNPs surface with DTSP.

Results shown in **Fig. 5a** reveal changes in both θ and δE parameters related to the chemical modification of the NPs surrounding medium. The strongest change in the $\langle \varepsilon_i \rangle$ spectra is observed after the covalent bonding of the anti-GSH to the DTSP layer, as this biomolecule is considerably larger in size than the DTSP molecule.

In order to determine the optimal amount of the antibody in the immunosensing layer, samples are exposed to different concentrations of anti-GSH from 25 to 600 nM. Results are represented in **Fig. 5b**. As the anti-GSH concentration increases, the δE undergoes a larger redshift, proportional to the surface coverage, until reaching a plateau when the DTSP binding sites on the GaNPs are saturated. This curve is optimally fitted to a Langmuir isotherm using:

$$\delta E = \frac{\delta E_{\max} \cdot K_L \cdot c}{1 + K_L \cdot c} \quad (6)$$

This function accounts for the formation of a monolayer. δE_{\max} , K_L and c are the maximum energy shift, the Langmuir constant and the antibody concentration, respectively. Using δE_{\max} , K_L as fitting parameters, best-fitting values of 146 meV and 0.014 are obtained for δE_{\max} , K_L , respectively. To prevent unnecessary reactive consumption, an antibody concentration of 150 nM is chosen for the final sensor preparation, since the value is in the plateau where higher concentrations would hardly improve the response, whereas lower concentrations could reduce GSH recognition sites and, thus, sensor sensitivity.

In order to assess the success of the GaNP functionalization with DTSP and the antibody immobilization, we perform FTIR spectra (Fig. 5c) under diffuse reflectance configuration for DTSP/GaNPs and anti-GSH/DTSP/GaNPs. All spectra are referenced to the spectrum obtained from as-evaporated GaNPs (non-functionalized). After the functionalization with DTSP (black curve), the C=O symmetric stretching mode, $\nu_s(\text{CO})$, at 1747 cm^{-1} can be identified. The typical amide bands are evident after the antibody immobilization (red curve). The amide I band, centered at 1684 cm^{-1} , (C=O and C-N symmetric stretching modes, $\nu_s(\text{CO})$ and $\nu_s(\text{CN})$) and the amide II band, centered at 1546 cm^{-1} , (N-H in-plane bending and C-N symmetric stretching modes, $\delta(\text{NH})$ and $\nu_s(\text{CN})$) (Parker 2012). The broad band observed in all spectra in the $3100\text{-}3400 \text{ cm}^{-1}$ range can be attributed to $\nu(\text{-OH})$ vibrations, likely caused by adsorbed water molecules. After the antibody immobilization, this broad band can overlap with those modes found for amine groups [$\nu_s(\text{NH})$ and $\nu_{\text{as}}(\text{NH})$].

From this analysis, we can conclude that the GaNP surface has been successfully functionalized. It is worth noticing that the bands are weak because the DTSP and the antibody typically form very thin layers with thicknesses of a few nanometers.

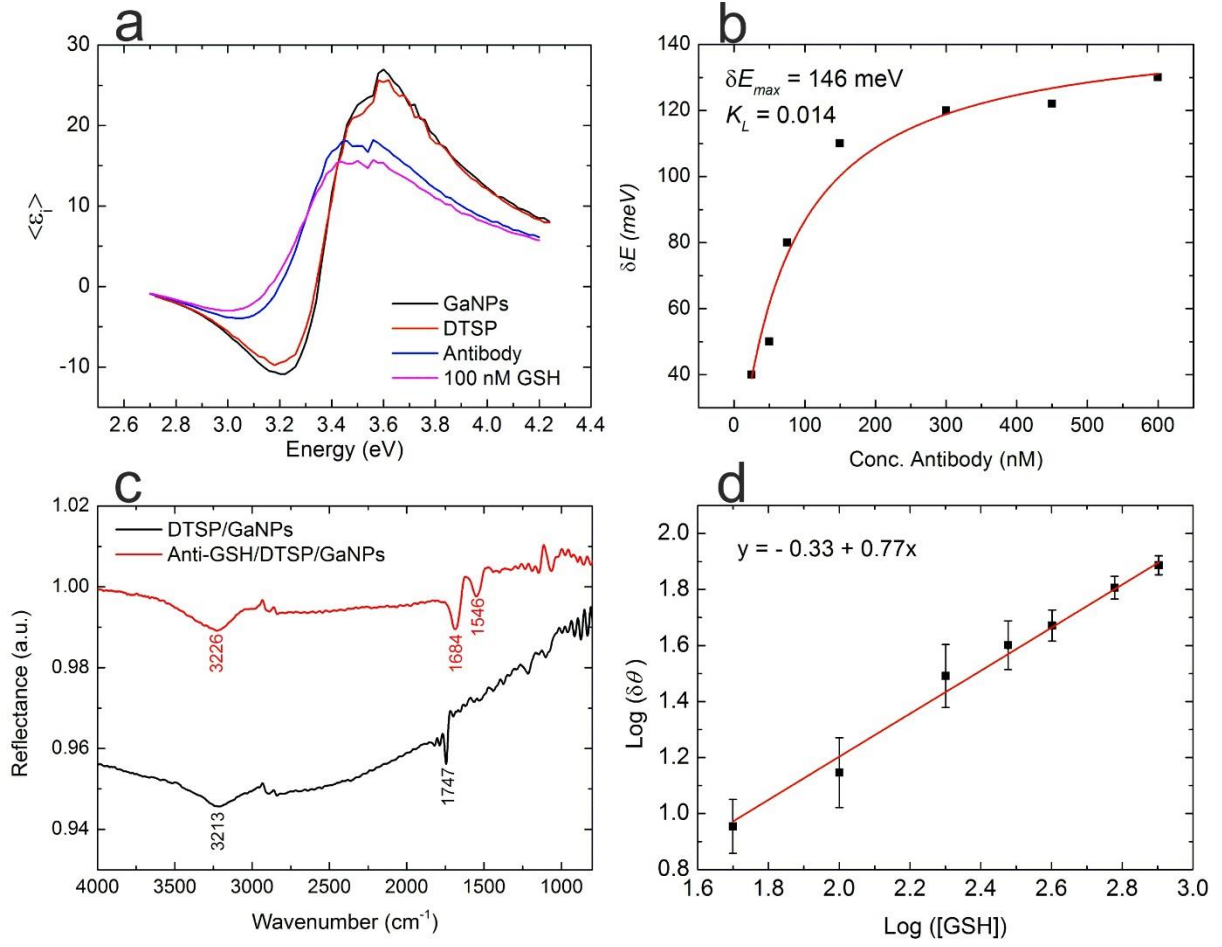


Fig. 5. (a) $\langle \varepsilon_i \rangle$ obtained at each preparation stage: as-deposited GaNPs, after DTSP modification, after antibody immobilization and after its exposure to 100 nM GSH (black, red, blue and magenta curves, respectively). (b) Experimental energy shifts of the RPH condition and Langmuir isotherm fitting for antibody concentrations between 25 and 600 nM. (c) FTIR spectra of DTSP/GaNPs and anti-GSH/DTSP/GaNPs surfaces. (d) Calibration curve for GSH sensing obtained from the variations in the slope of $\langle \varepsilon_i \rangle$ at the RPH condition ($\delta\theta$); error bars represent the standard deviation of measurements from three different immunosensors.

To evaluate the immunosensing response of the anti-GSH GaNP nanostructured surface, the sample is incubated in a solution of 100 nM GSH for 1 hour. After rinsing the sample with deionized water and blowing its surface with dry nitrogen, a reduction of the peak-to-peak amplitude in $\langle \varepsilon_i \rangle$ around the RPH condition is found (**Fig. 5a**). This reduction is easily quantified by measuring the slope at the RPH condition, θ . In general, this parameter has shown

more sensitivity than the energy shift of the RPH condition to changes in the NP surrounding medium. The parameter is particularly useful for sensing a small biomolecule like the GSH. Therefore, the GSH sensor is developed from the variations measured in the slope of $\langle \varepsilon_i \rangle$ at the RPH condition ($\delta\theta$).

Unspecific bonding of the GSH to the DTSP-functionalized GaNPs is also studied. For this purpose, a DTSP-functionalized GaNPs without anti-GSH is immersed in an aqueous solution of 0.01 M of KCl for 3 hours. The ellipsometric response of this chip after its incubation with 400 nM of GSH for 1 h does not show any significant change. From this experiment, it can be concluded that the changes measured in the $\langle \varepsilon_i \rangle$ spectra after incubation of the immunosensor in the GSH solution are due to the specific interaction between the antibody and the GSH.

On the basis of the above results, the immunosensor response to GSH is obtained following the θ changes caused by the GSH recognition through the active sites of the antibody. Different immunosensor chips, prepared by the same manner, are incubated for 1 hour in solutions containing increasing concentrations of GSH from 50 to 800 nM. The incubation time is chosen according to previous results obtained in a kinetic study performed between the same antibody and analyte, from which it was concluded that 35 min are enough to ensure that the binding process reaches the equilibrium (García-Marín et al. 2014).

Fig. 5d shows the immunosensor response obtained by plotting $\log(\delta\theta)$ as a function of $\log([GSH])$, with $\delta\theta$ and $[GSH]$ expressed in eV^{-1} and nM units, respectively. In this figure, the $\delta\theta$ changes are calculated by subtracting the slope variation in a blank sample, only treated with deionized water, to the slope variation obtained for each concentration of GSH in the $\langle \varepsilon_i \rangle$ spectra. Each data point in the curve represents the average value of measurements taken from three different immunosensors. A good linear correlation is observed in the 50 to 800 nM concentration range ($R^2 = 0.998$). The limits of detection and quantification are 10 nM (0.003

$\mu\text{g/mL}$) and 50 nM (0.015 $\mu\text{g/mL}$), calculated as the ratio between three and ten times the standard deviation of the background signal and the sensitivity, respectively. These values represent an improvement compared to the sensitivity of standard ELISA kits available in the market (see reference list), whose minimum GSH concentration detected is between 0.1 and 0.5 $\mu\text{g/mL}$.

The repeatability is evaluated from the relative standard deviation (RSD) of three successive determinations with the same immunosensor. A RSD value of 0.4% is obtained. The reproducibility for 400 nM GSH using three different immunosensors is 6%. Finally, the storage stability is studied, concluding that the immunosensor retains about 95% of its initial response after 8 days, keeping it under refrigeration ($< 4^{\circ}\text{C}$).

For the sake of comparison, a table including the results obtained by other GSH sensing methods is provided in the supporting information (Table S1). Our method compares well with those previously described. In general, those publications that report a lower limit of detection require two functionalization protocols, one for the sensing surface and another one for additional nanostructures that act as signal amplifiers. For instance, the methods described by Stobiecka et al. (Stobiecka and Hepel 2011) and García-Marín et al. (García-Marín et al. 2014) use gold nanoparticles to enhance the sensitivity after the previous immobilization of the analyte on the NP surface, which can hinder GSH quantification in more complex matrices.

4. Conclusions

In conclusion, the feasibility of GSH immunosensors based on the ellipsometric analysis of GaNPs/Si platforms around the RPH condition is demonstrated. This condition appears near the higher energy resonant mode of GaNPs, producing a characteristic line-shape in the imaginary part of the pseudodielectric function at energies of 2.6-3.5 eV under an incidence angle of 55° . The immunosensing chips are fabricated from GaNPs evaporated on Si substrates.

Obtaining these close-packed arrays directly by thermal evaporation without any additional treatment demonstrates the cost-effectiveness of this procedure.

GaNP surface is further functionalized with a layer of antibodies against GSH. A relationship between the GSH concentration and the slope in $\langle \varepsilon_i \rangle$ at the RPH experimental conditions is found through its interaction with the antibody, providing limits of detection in the nanomolar range. It is worth noting that the use of these GaNP nanostructured surfaces could be extended to the development of different analyte sensors, such as DNA or proteins, by simply changing the recognition element.

Acknowledgements

The authors thank Dr. M. Cervera for his assistance in ellipsometric measurements. This research is partially supported by the Ministry of Economy and Competitiveness (CTQ2014-53334-C2-1-R and 2-R) and Comunidad de Madrid (NANOAVANSENS ref. S2013/MIT-3029).

References

- ELISA commercial kits for glutathione: <http://www.biomatik.com/products/productDetail/ELISA-Kit-for-Glutathione--GSH---General--competitive-type.aspx>, <http://www.uscnk.com/uscn/ELISA-Kit-for-Glutathione-GSH-1197.htm>, (accessed May, 2015).
- Aćimović, S.S., Ortega, M.A., Sanz, V., Berthelot, J., Garcia-Cordero, J.L., Renger, J., Maerkl, S.J., Kreuzer, M.P., Quidant, R., 2014. *Nano Lett.* 14, 2636–2641.
- Albella, P., Garcia-Cueto, B., González, F., Moreno, F., Wu, P.C., Kim, T.-H., Brown, A., Yang, Y., Everitt, H.O., Videen, G., 2011. *Nano Lett.* 11, 3531–3537.
- Appenzeller-Herzog, C., 2011. *J Cell. Sci.* 124, 847–855.
- Buttke, T.M., Sandstrom, P.A., 1994. *Immunol. Today* 15, 7–10.
- Campbell, C.T., 1997. *Surf. Sci. Rep.* 27(1–3), 1–111.
- Darder, M., Takada, K., Pariente, F., Lorenzo, E., Abruña, H.D., 1999. *Anal. Chem* 71, 5530–5537.
- Eustis, S., El-Sayed, M.A., 2006. *Chem. Soc. Rev.* 35(3), 209–217.
- Galera, R.M.L., Giménez, J.C.J., Ronsano, J.B.M., Cardona, R.M.S., Via, M.A.A., Roca, C.A., Puigbert, J.M.T., 1996. *Clin. Chim. Acta* 254, 63–72.
- García-Marín, A., Abad, J.M., Ruiz, E., Lorenzo, E., Piqueras, J., Pau, J.L., 2014. *Anal. Chem.* 86, 4969–4976.
- Gerdon, A.E., Wright, D.W., Cliffel, D.E., 2005. *Anal. Chem.* 77, 304–310.

Gutscher, M., Pauleau, A.L., Marty, L., Brach, T., Wabnitz, G.H., Samstag, Y., Meyer, A.J., Dick, T.P., 2008. *Nat. Methods* 5, 553-559.

Harfield, J.C., Batchelor-McAuley, C., Compton, R.G., 2012. *Analyst* 137(10), 2285-2296.

Hedley, D.W., Chow, S., 1994. *Cytometry* 15, 349-358.

Hernández, M.J., Cervera, M., Ruiz, E., Pau, J.L., Piqueras, J., Avella, M., Jiménez, J., 2010. *Nanotech.* 21, 455602.

Homola, J., 2003. *Anal. Bioanal. Chem.* 377, 528-539.

Homola, J., Yee, S.S., Gauglitz, G., 1999. *Sens. Actuators B Chem.* 54, 3-15.

Kataoka, H., Takagi, K., Makita, M., 1995. *Biomed. Chromatogr.* 9, 85-89.

Knight, M.W., Coenen, T., Yang, Y., Brenny, B.J.M., Losurdo, M., Brown, A.S., Everitt, H.O., Polman, A., 2015. *ACS Nano* 9(2), 2049-2060.

Lodewijks, K., Roy, W.V., Borghs, G., Lagae, L., Dorpe, P.V., 2012. *Nano Lett.* 12, 1655-1659.

Lu, C., Zu, Y., Yam, V.W.W., 2007. *J. Chromatogr. A* 1163, 328-332.

Lusini, L., Tripodi, S.A., Rossi, R., Giannerini, F., Giustarini, D., Vecchio, M.T.d., Barbanti, G., Cintorino, M., Tosi, P., Simplicio, P.D., 2001. *Int. J. Cancer* 91, 55-59.

May, M.J., Vernoux, T., Leaver, T., Van Montagu, M., Inzé, D., 1998. *J. Exp. Bot.* 49, 649-667.

Mayatepek, E., Jaeken, J., 2012. *Inborn Metabolic Diseases*, 423-430.

Meister, A., 1983. *Science* 220, 472-477.

Meister, A., 1988. *J. Biol. Chem.* 263, 17205-17208.

Meister, A., Anderson, M.E., 1983. *Annu. Rev. Biochem.* 52, 711-760.

Meyer, A.J., May, M.J., Fricker, M., 2001. *The Plant Journal*. 27, 67-78.

Michieli, N., Kalinic, B., Scian, C., Cesca, T., Mattei, G., 2015. *Biosens. Bioelectron.* 65(0), 346-353.

Morrison, J.A., Jacobsen, D.W., Sprecher, D.L., Robinson, K., Khoury, P., Daniels, S.R., 1999. *Circulation* 100(22), 2244-2247.

Ndamanisha, J.C., Bai, J., Qi, B., Guo, L., 2009. *Anal. Biochem.* 386, 79-84.

Parker, F., 2012. *Applications of Infrared Spectroscopy in Biochemistry, Biology, and Medicine*. Springer.

Pocernich, C.B., D. A. Butterfield, 2012. *Biochim. Biophys. Acta* 1822, 625-630.

Ruan, E.A., Rao, S., Burdick, J.S., Stryker, S.J., Telford, G.L., Otterson, M.F., Opara, E.C., Koch, T.R., 1997. *Nutr. Res.* 17, 463-473.

Schasfoort, R.B.M., Tudos, A.J., 2008. *Handbook of surface plasmon resonance*. RSC Publishing, Cambridge.

Sies, H., 1999. *Free Radic. Biol. Med.* 27, 916-921.

Stobiecka, M., Hepel, M., 2011. *Biosens. Bioelectron.* 26(8), 3524-3530.

Tompkins, H.G., 1993. *A User's Guide to Ellipsometry*. Academic Press.

Tonova, D., Patrini, M., Tognini, P., Stella, A., Cheyssac, P., Kofman, R., 1999. *J. Phys.: Condens. Matter* 11, 2211-2222.

Vacek, J., Klejdus, B., Petřlová, J., Lojková, L., Kubá, V., 2006. *Analyst* 131, 1167-1174.

Verre, R., Modreanu, M., Ualibek, O., Fox, D., Fleischer, K., Smith, C., Zhang, H., Pemble, M., McGilp, J.F., Shvets, I.V., 2013. *Phys. Rev. B* 87(23), 235428.

Viswambari Devi, R., Doble, M., Verma, R.S., 2015. *Biosens. Bioelectron.* 68(0), 688-698.

Wagner, P., Hegner, M., Kernen, P., Zaugg, F., Semenza, G., 1996. *Biophys. J.* 70, 2052-2066.

White, P.C., Lawrence, N.S., Davis, J., Compton, R.G., 2002. *Electroanal.* 14, 89-98.

Willems, K.A., Duyne, R.P.V., 2007. *Annu. Rev. Phys. Chem.* 58, 267-297.

Wu, P.C., Kim, T.-H., Brown, A.S., Losurdo, M., Bruno, G., Everitt, H.O., 2007. *Appl. Phys. Lett.* 90, 103119.

Wu, P.C., Losurdo, M., Kim, T.-H., Giangregorio, M., Bruno, G., Everitt, H.O., Brown, A.S., 2009. *Langmuir* 25, 924-930.

Xu, C., Li, H., Yin, B., 2015. *Biosens. Bioelectron.* 72(0), 275-281.

Yang, Y., Callahan, J.M., Kim, T.-H., Brown, A.S., Everitt, H.O., 2013. *Nano Lett.* 13, 2837-2841.

Zhang, W., Wan, F., Zhu, W., Xu, H., Ye, X., Cheng, R., Jin, L.-T., 2005. *J. Chromatogr. B* 818, 227-232.